

Ocean-driven thinning enhances iceberg calving and retreat of Antarctic ice shelves

Yan Liu^{a,b}, John C. Moore^{a,b,c,d,1}, Xiao Cheng^{a,b,1}, Rupert M. Gladstone^{e,f}, Jeremy N. Bassis^g, Hongxing Liu^h, Jiahong Wenⁱ, and Fengming Hui^{a,b}

^aState Key Laboratory of Remote Sensing Science, College of Global Change and Earth System Science, Beijing Normal University, Beijing 100875, China; ^bJoint Center for Global Change Studies, Beijing 100875, China; ^cArctic Centre, University of Lapland, 96100 Rovaniemi, Finland; ^dDepartment of Earth Sciences, Uppsala University, Uppsala 75236, Sweden; ^eAntarctic Climate and Ecosystems Cooperative Research Centre, University of Tasmania, Hobart, Tasmania, Australia; ^fVersuchsanstalt für Wasserbau, Hydrologie und Glaziologie, Eidgenössische Technische Hochschule Zürich, 8093 Zurich, Switzerland; ^gDepartment of Atmospheric, Oceanic and Space Sciences, University of Michigan, Ann Arbor, MI 48109-2143; ^hDepartment of Geography, McMicken College of Arts & Sciences, University of Cincinnati, OH 45221-0131; and ⁱDepartment of Geography, Shanghai Normal University, Shanghai 200234, China

Edited by Anny Cazenave, Centre National d'Etudes Spatiales, Toulouse, France, and approved February 10, 2015 (received for review August 7, 2014)

Iceberg calving from all Antarctic ice shelves has never been directly measured, despite playing a crucial role in ice sheet mass balance. Rapid changes to iceberg calving naturally arise from the sporadic detachment of large tabular bergs but can also be triggered by climate forcing. Here we provide a direct empirical estimate of mass loss due to iceberg calving and melting from Antarctic ice shelves. We find that between 2005 and 2011, the total mass loss due to iceberg calving of 755 ± 24 gigatonnes per year (Gt/y) is only half the total loss due to basal melt of 1516 ± 106 Gt/y. However, we observe widespread retreat of ice shelves that are currently thinning. Net mass loss due to iceberg calving for these ice shelves (302 ± 27 Gt/y) is comparable in magnitude to net mass loss due to basal melt (312 ± 14 Gt/y). Moreover, we find that iceberg calving from these decaying ice shelves is dominated by frequent calving events, which are distinct from the less frequent detachment of isolated tabular icebergs associated with ice shelves in neutral or positive mass balance regimes. Our results suggest that thinning associated with ocean-driven increased basal melt can trigger increased iceberg calving, implying that iceberg calving may play an overlooked role in the demise of shrinking ice shelves, and is more sensitive to ocean forcing than expected from steady state calving estimates.

iceberg calving | basal melt | mass balance | ice shelf | Antarctica

The majority of Antarctica's mass loss to the ocean occurs through its fringing ice shelves via iceberg calving and basal melt (1–3). Although the mass balance of ice shelves has a negligible direct effect on sea level rise (because the ice shelves float freely), the ice shelves buttress the grounded ice upstream and have been shown to play a major role in stabilizing the discharge of grounded ice to the ocean (4–6). Reduction of buttressing due to increased iceberg calving or basal melt leads to thinning and acceleration of inland glaciers (4–7), and may be driven by regional and global changes in atmospheric and oceanic conditions through ice–ocean and ice–atmosphere interactions (4, 5, 7–11). Catastrophic ice shelf disintegration driven by atmospheric warming has led to abrupt ice shelf retreat in the Antarctic Peninsula (5, 11), which, combined with basal melt induced thinning, has contributed to the 34% increased discharge of grounded ice to the ocean from West Antarctica from 1996 to 2006 (6).

The mass balance of an ice shelf is determined by the difference between mass gained from the flux of ice across the grounding line into the ice shelf, deposition of snow on the surface or marine ice on the bottom of the ice shelf, and mass lost by melting (surface and basal) and iceberg calving. In steady state, the ice shelf has no areal extent change (steady-state calving front) and no thickness change (steady-state ice thickness). It is possible to define a steady-state basal melt (or marine ice accretion) necessary to maintain steady-state ice thickness for given cross-grounding line fluxes, surface mass balance, and calving fluxes (2). Similarly, the steady-state iceberg calving is

defined as the calving flux necessary to maintain a steady-state calving front for a given set of ice thicknesses and velocities along the ice front gate (2, 3). Estimating the mass balance of ice shelves out of steady state, however, requires additional information about the change of ice thickness and the change of areal extent of the ice shelf, which is determined by the advance or retreat of the calving front. Several recent studies have sought to estimate the nonsteady-state mass balance of ice shelves at broad scales (2, 3, 12), but these studies indirectly inferred iceberg calving assuming a steady-state calving front, neglecting the contribution of advance or retreat of the calving front to the mass balance of ice shelves (2, 3). Such “flux gate” calculations are inevitably biased, as they underestimate iceberg calving for retreating ice shelves or overestimate it for advancing ice shelves. This deficiency is problematic not only for estimates of the mass balance of ice shelves but also because current models of iceberg calving provide conflicting predictions about whether increased basal melt will lead to an increase or decrease in iceberg calving (1, 13–15).

Here we avoid the assumption of steady-state calving front by combining traditional estimates of ice shelf mass balance with an annual record of iceberg calving events larger than 1 km^2 from all Antarctic ice shelves exceeding 10 km^2 in area for the period 2005–2011. Our observations show that both iceberg calving (Fig. 1) and ice shelf extent (Fig. 2) change over the observational period, proving that the steady-state calving front assumption is invalid. To estimate mass loss due to iceberg calving, we manually

Significance

The floating parts of the Antarctic ice sheet (“ice shelves”) help to hold back the flow of the grounded parts, determining the contribution to global sea level rise. Using satellite images, we measured, for the first time, all icebergs larger than 1 km^2 calving from the entire Antarctic coastline, and the state of health of all the ice shelves. Some large ice shelves are growing while many smaller ice shelves are shrinking. We find high rates of iceberg calving from Antarctic ice shelves that are undergoing basal melt-induced thinning, which suggests the fate of ice shelves may be more sensitive to ocean forcing than previously thought.

Author contributions: Y.L., J.C.M., and X.C. designed research; Y.L. and F.H. performed research; Y.L., J.C.M., X.C., R.M.G., J.N.B., H.L., J.W., and F.H. contributed new reagents/analytic tools; Y.L., J.C.M., X.C., R.M.G., J.N.B., H.L., J.W., and F.H. analyzed data; and Y.L., J.C.M., X.C., R.M.G., J.N.B., H.L., and J.W. wrote the paper.

The authors declare no conflict of interest.

This article is a PNAS Direct Submission.

Freely available online through the PNAS open access option.

¹To whom correspondence may be addressed. Email: xcheng@bnu.edu.cn or john.moore.bnu@gmail.com.

This article contains supporting information online at www.pnas.org/lookup/suppl/doi:10.1073/pnas.1415137112/-DCSupplemental.

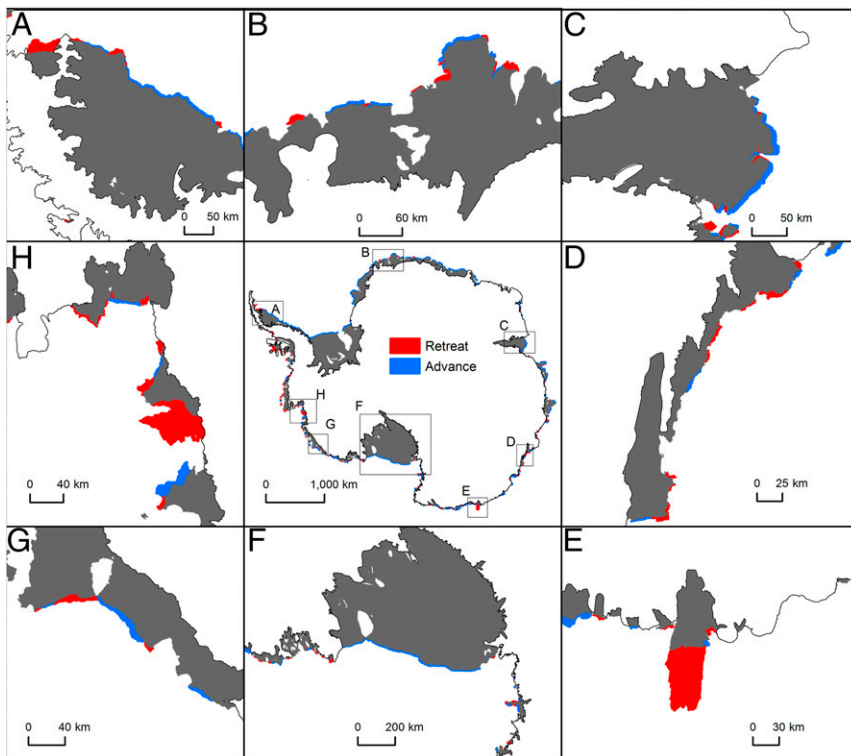


Fig. 2. Antarctic ice shelf advance and retreat between 2005 and 2011. (A) Larsen B and C Ice Shelf; (B) Fimbulisen, Jelbartisen, and Ekströmsen Ice Shelf; (C) Amery Ice Shelf; (D) Totten and Moscow University Ice Shelf; (E) Mertz Glacier Tongue; (F) Ross Ice Shelf; (G) Getz Ice Shelf; and (H) the floating parts of Pine Island and Thwaites Glaciers, and Crosson Ice Shelf.

Surprisingly, other disintegration events that we observe occurred in colder environments with little or no evidence for surface melt. These events typically occurred in regions with large-scale visible rift and crevasse zones and a rapidly flowing ice front (Fig. 3C) and are difficult to detect because the readvance of the ice front partially obscures the change in calving front position.

In conjunction with quantifying iceberg calving, we also developed a flow-line method to quantify cross-grounding line fluxes for the whole of Antarctica (*Materials and Methods*). Using these techniques, we provide an estimate of Antarctic ice shelf mass balance that is not constrained by the steady-state assumption. The mass balance of ice shelves is presented both in terms of volumetric components (net ice shelf volume change

due to thickness and extent changes) and its budget components (surface mass balance, cross-grounding line fluxes, iceberg calving, and basal melt). Moreover, steady-state iceberg calving and steady-state basal melt are also estimated and agree well with previous estimates (2, 3) (*Tables S1* and *S2*). We calculated all these components and associated uncertainties for 7 large drainage systems (Filchner-Ronne, East Antarctica KB, Amery, East Antarctica CE, Ross, West Antarctica, and Peninsula), 26 basin systems labeled A~K, and 94 subbasin systems covering the entire continent (Fig. 1 and *Dataset S1*).

We find that the mean annual mass balance of all Antarctic ice shelves is slightly positive (46 ± 41 Gt/y) between 2005 and 2011, but with large interannual variability because of the irregular

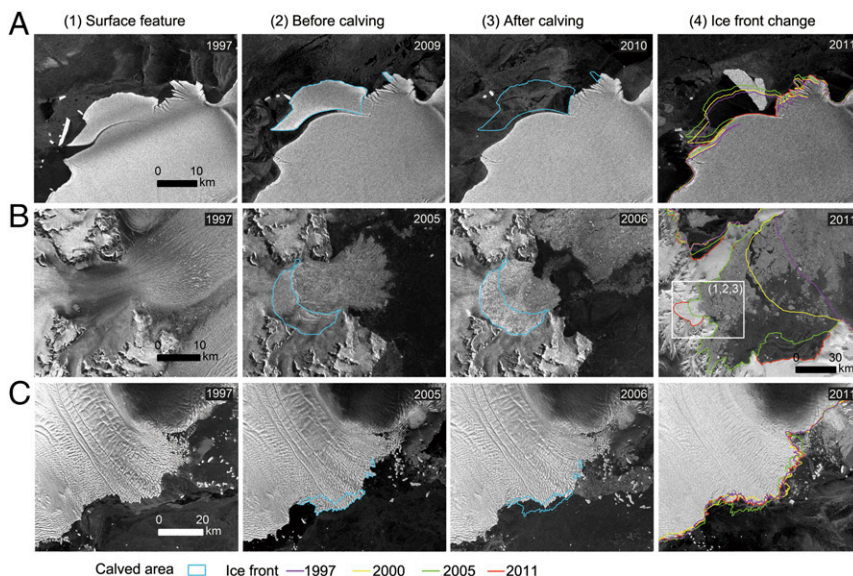


Fig. 3. Different calving features. (A) Example of tabular calving from the Fimbulisen Ice Shelf, (B) example of melt pond induced disintegration from the Larsen B ice shelf, and (C) example of crevasse induced disintegration from the Totten glacier. (1) Calving feature on synthetic aperture radar image in 1997 (bright white ponds shown in B image are melt ponds). ENVISAT ASAR image with area calved marked before (2) and after (3) calving. (4) Ice front changes overlaid on Envisat ASAR image in 2011.

Table 1. Mean mass balance of Antarctic ice shelves in different state during 2005–2011

Components	State of ice shelf mass balance			
	Negative	Near-zero	Positive	Total
Number of subbasin systems	33	17	43	93*
Total ice shelf area, km ²	284,292	98,522	1,159,293	1,542,108
Ice shelf mass balance, Gt/y	-614 ± 34	4 ± 6	655 ± 37	46 ± 41
Volumetric components, Gt/y				
Mass change due to thickness change	-312 ± 14	-20 ± 5	107 ± 25	-226 ± 25
Mass change due to extent change	-302 ± 27	24 ± 3	549 ± 27	271 ± 21
Budget components, Gt/y				
Grounding line flux	929 ± 60	203 ± 10	838 ± 41	1970 ± 75
Surface mass balance	116 ± 9	30 ± 2	200 ± 9	346 ± 37
Steady-state basal melt	706 ± 92	180 ± 13	405 ± 63	1290 ± 110
Basal melt	1018 ± 90	200 ± 12	298 ± 58	1516 ± 106
Steady-state iceberg calving	339 ± 30	53 ± 4	633 ± 29	1026 ± 39
Iceberg calving	641 ± 24	29 ± 3	84 ± 7	755 ± 25

*One of the 94 subbasin systems has no ice shelf larger than 10 km².

occurrence of extralarge-size (larger than 1,000 km²) calving events (Table 1 and Fig. 4A). Our calculated basal melt of 1516 ± 106 Gt/y accounts for two thirds of Antarctic ice shelf total mass loss while iceberg calving of 755 ± 25 Gt/y accounts for the remaining third (Table 1). The total contribution of iceberg calving to the mass balance might be much higher if the records of infrequent large iceberg detachment are extended by several decades. For example, a sequence of major calving events such as those that detached from the Amery Ice Shelf in 1963–1964 (17) or from the Ross and Filchner-Ronne Ice Shelf in 2001–2002 (20), would result in a (temporary) net negative mass balance for Antarctic ice shelves. We detect 579 distinct iceberg calving events, ranging in size from 1 km² to 3,115 km² over the 7-y study period. As we have data at monthly resolution for only 3 y (15), the calving events we detect may have resulted from either a sequence of several separate calving events or a single larger calving event. Only three cases larger than 1,000 km² are detected: the calving of the Mertz Ice Tongue by iceberg collision (21); the calving of the floating part of Thwaites Glacier by progressive rifting (10); and the disintegration of the Wilkins Ice Shelf, possibly caused by ocean-driven basal melt (19). However, 95% of calving events are small and medium in scale (1–100 km² in size), accounting for about 38% of total calving mass over the 7-y study (Tables S3 and S4).

In contrast with recent studies suggesting most ice shelves are close to steady state (3), our basal melt and iceberg calving results (Table 1 and Fig. 4B) indicate significant mass imbalance in more than three quarters of ice shelf subbasin systems. We find two opposing regimes or patterns of mass loss around Antarctica. There are 43 ice shelf subbasin systems in positive mass balance, and, for these ice shelves, basal melt and calving are just 74% ($P < 0.1$ in Student's t test) and 13% ($P < 0.001$), respectively, of their inferred steady-state values (Table 1 and Fig. 4C). Most calving events on these ice shelves produce infrequent, isolated tabular icebergs (Fig. 3A and Fig. S1) and do not reoccur at the same location during our observation period (1997–2011). This previously documented tabular calving style is thought to be primarily controlled by internal stress and characterized by a natural cycle with several decades of quiescence between major calving events (13, 16–18).

There are 33 ice shelf subbasin systems in negative mass balance, but they account for only about 18% of total ice shelf area. These subbasins account for 73% of the total mass loss, comprising 67% of total Antarctic ice shelf basal meltwater production (1018 ± 90 Gt/y) and 85% of total calving (641 ± 43 Gt/y). For these ice shelves, basal melt and calving are 144%

($P < 0.01$) and 189% ($P < 0.01$), respectively, of their steady-state values. Twenty-four of these subbasins experienced both ice shelf retreat and thinning (Dataset S1). We note that the “increased” basal melt we report is referenced relative to our inferred steady-state basal melt and hence, by definition, leads to ice shelf thinning. Similarly, the enhanced iceberg calving is also relative to the steady-state calving required to maintain a constant calving front position and hence “enhanced” calving leads to ice shelf retreat and area loss. Thus, the negative mass balance of these ice shelves results not only from increased basal melt (2, 3, 12) but also from increased iceberg calving. Contributions to the net mass loss from ice shelf thinning and calving front retreat are similar (Table 1). This is true even for the floating parts of Pine Island and Thwaites Glaciers, which are among the best-studied on the continent (22). Both of these ice tongues calved large (larger than 500 km²) tabular icebergs twice between 1997 and 2011. However, they experienced more frequent sequences of smaller-scale calving events, typically of less than 100 km² (Fig. S1 and Table S3). This mode of calving, associated with rapid-flowing ice fronts and intense crevassing and rifting (e.g., Fig. 3C), is common to many of the retreating ice shelves we

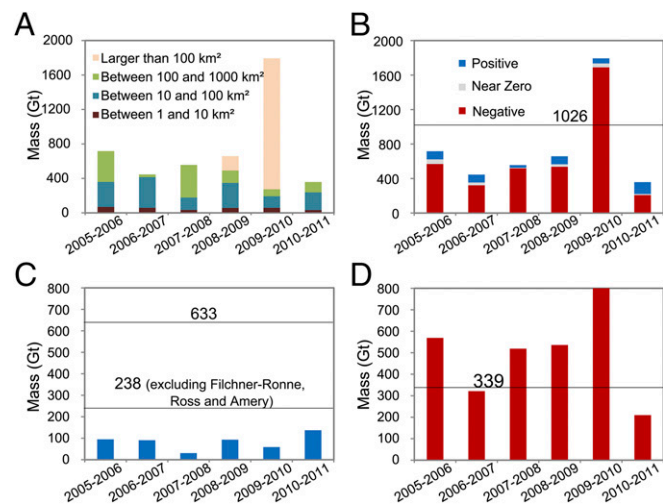


Fig. 4. Annual Antarctic iceberg calving from 2005 to 2011. (A) All ice shelves by calving size; (B) calving by state of mass balance; (C) ice shelves in positive mass balance; and (D) ice shelves in negative mass balance. Horizontal lines in B, C, and D denote steady-state iceberg calving for those ice shelves.

observed. These frequent calving events have been overlooked by previous studies, which assumed that calving is dominated by infrequent tabular berg calving. The calving front retreat associated with ice shelves in negative mass balance has a robustly identifiable trend over our study period (Fig. 4D) due to the shorter recurrence intervals typical of these more frequently calving systems. However, calving (and basal melting) may also vary over decadal and longer time scales not captured by our limited observational period.

The ice shelves undergoing calving front advance and/or ice thickening are the large ice shelf drainage systems (Filchner-Ronne, Ross, and Amery Ice Shelf) together with the neighboring systems of I'J, D'E, and KA', in the Ross Sea, Weddell Sea, and Indian Ocean regions (Fig. 2). These ice shelves account for 78% of the entire Antarctic ice shelf area. They have a positive or near-zero mass balance and are located at high southern latitudes or are fed by an ice sheet grounded well above sea level. These regions are both cold and continental in character and have low net snow accumulation. For some sections of these ice shelves, basal freezing occurs (Fig. 2), which often coincides with observed marine ice "stripes" (23). Marine ice is softer than meteoric ice and has been hypothesized to play an important role in filling and healing bottom crevassing along shear zones, hence determining ice shelf durability (and length of calving cycles) (24–26).

The ice shelves in negative mass balance are primarily small to medium ice shelves located around the Antarctic Peninsula (H'I) and West Antarctica in the Bellingshausen/Amundsen Seas, and East Antarctica along the Wilkes Land coastline (C'D) (Fig. 2, Fig. S1, Dataset S1, and Table S3). The ice shelves in negative mass balance of the Antarctic Peninsula are fed locally, have small grounding line fluxes, and have thinner than average ice fronts (Fig. 2 and Dataset S1). The presence of surface meltwater ponds due to rising atmospheric temperatures has led to catastrophic disintegration events (8, 27), which have only occurred, to date, on the Antarctic Peninsula (24). However, basal melt much larger than necessary to maintain a steady-state ice thickness may have also contributed to the demise of Antarctic Peninsula ice shelves. For example, basal melt exceeded ice flux across the grounding line after 2005 for the more southerly located Wilkins Ice Shelf (Dataset S1), suggesting that it experienced high ocean-driven thinning before disintegration. The southern edge of George VI Ice Shelf is also experiencing increased basal melt and is undergoing similar, but localized, disintegration (7). Increased basal melt driven by warmer water masses beneath the shelves could also diminish or even halt marine ice formation within suture zones that occur in colder ocean environments, reducing the stabilizing effect on basal fractures, and ice shelf structural integrity (25, 26, 28).

The ice shelves in negative mass balance of the West Antarctic systems F'H' and East Antarctic systems C'D' are mostly fed by marine based glaciers grounded well below sea level. The rapid response time of these high-throughput systems, which experience high surface accumulation and basal melt (3), may be further increased by the marine ice sheet instability (1) and associated feedbacks. This results in small and potentially vulnerable ice shelves. The presence of both ice shelf thinning and retreat in this region (Dataset S1) hint at a connection between increased basal melt and enhanced iceberg calving. Warm Circumpolar Deep Water (CDW), or slightly modified CDW, lies just off the continental shelf break in these regions (29). Thoma et al. (30) postulated that wind-driven increases in upwelling drive CDW over the continental shelf break and into ice shelf cavities, increasing basal melt and leading to the pronounced observed ice shelf thinning (11, 30, 31). While the relationship between increased basal melt and ocean forcing is clear, it is less clear whether the observed enhanced iceberg calving is simply a direct result of ice shelf thinning or is driven by more complex subshelf processes. It is possible that pronounced and spatially varying basal melt can undercut the submerged ice fronts (9).

Additionally, increased melting of ice mélange, a mixture of sea ice, snow, ice shelf fragments, and marine ice trapped in between the rifts may accelerate rift propagation and threaten ice shelf stability (32, 33). Large-scale crevasse-like surface features are common on the ice shelves along F'H and C'D'. Recent observations from ground-penetrating radar show that many of these are, in fact, the surface expression of deep and wide transverse basal crevasses (13, 34) or longitudinal subglacial melt channels (35). The basal channels or crevasses can be incised 200 m into the ice shelf base (34, 35), and the surface depressions can be more than 30 m lower than the usual ice shelf surface (36), making the features the thinnest regions of the ice shelves. These crevasse-like features may provide multiple sites for potential full-thickness crevassing and rift opening. Models show that the tensile stress induced by these wide basal channels is sufficient to cause additional surface and basal crevasse propagation (34, 35). Increased basal melt may enhance this process, as the thinner shelf will flex more and increase the likelihood of full-thickness rift formation (35). For example, Totten Glacier is an ice shelf that has experienced thinning due to increased basal melt, and we observe calving associated with surface troughs (Fig. 3C). These crevasse-like zones cover a considerable area of ice shelves in the F'H' and C'D' regions, potentially rendering many Antarctic ice shelves susceptible to massive, catastrophic disintegrations in the event of further increases in basal melt (15).

Given these results, we propose that ocean-driven increased basal melt enhances fracturing of Antarctic ice shelves. We also suggest that the numerous small ice shelves along the Antarctic Peninsula, Amundsen Sea Embayment, and Wilkes Land that have experienced marked increases in basal melt and iceberg calving over the past 2 decades may be poised for major retreat. This needs to be better understood so that it can be factored into future sea level projections.

Materials and Methods

The mass change of an ice shelf, ΔM , over a given time period, Δt , calculated in terms of volumetric components as the sum of change due to mean shelf thickness change, ΔM_H (negative for thinning), and change due to areal extent change (i.e., advance/retreat of ice front), ΔM_A (negative for retreat), is approximately given by a Taylor Series,

$$\Delta M = \Delta M_H + \Delta M_A = A_0 \Delta H \rho_i + H_0 \Delta A \rho_i \quad [1]$$

where ρ_i is the ice density, A_0 and ΔA are the reference area and change in area, H_0 and ΔH are the reference mean ice thickness and change in mean ice thickness, and we have neglected higher-order terms in the expansion. The reference values are based on the mean values from the 2005–2011 period. We combined the ice shelf area changes of Antarctic ice shelves in 2005–2011 with 2003–2011 ice thickness and 2003–2008 ice shelf thickness changes to estimate the Antarctic ice shelf mass balance. Ice shelf extent changes are identified by coregistered pairs of monthly ASAR data for August 2005 and August 2011. Ice thicknesses are estimated by combining the direct measurements in 2009–2011 from Multichannel Coherent Radar Depth Sounder (MCRDS) by Operation IceBridge mission with the indirect estimates in 2003–2009 from the Geoscience Laser Altimeter System (GLAS) instrument aboard ICESat (SI Materials and Methods). Average ice shelf thickness change for the period 2003–2008 is derived by the procedure in ref. 12 using ICESat-1 GLAS data.

The mass balance can also be expressed in terms of budget components in Gt/y.

$$\frac{\Delta M}{\Delta t} = F_G + SMB - C - B \quad [2]$$

where F_G is the integrated flux into the ice shelf across the grounding line (calculated using flux gates; see SI Materials and Methods), C is the rate of change of mass due to iceberg calving, SMB is the surface mass balance (the difference between surface accumulation and ablation rate), and B is the rate of change of mass due to basal melt (negative for freeze-on).

Cross-Grounding Line Flux. We use the Interferometric Synthetic Aperture Radar (InSAR) velocities and ice thicknesses at the flux gates to calculate

cross-grounding line flux F_G . Ice thicknesses are estimated by combining MCORDS data and ICESat GLAS data (*SI Materials and Methods*). Flux gates are positioned at the grounding line as determined by a combination of two published data sets. For the most part, the more accurate InSAR grounding line position is used, but where coverage is lacking, the grounding line from imagery and ICESat GLAS is used to achieve complete coverage. Cross-grounding line flux is determined using a flow-line routing algorithm (*SI Materials and Methods, Figs. S2 and S3*). Ice fluxes are estimated by ice flow across each unit of 900-m-width pixel at the grounding line. More than 20,000 flux units around Antarctica are calculated.

Surface Mass Balance. We use the surface mass balance product derived from a firm model UUFIRNMODELv3.1/ANT forced by climate data from RACMOv3.2/ANT27 for the period 2003–2008 (12).

Iceberg Calving. Iceberg calving is the actual rate of ice mass loss due to iceberg calving rather than a “flux gate” calculation (2, 3). It is calculated as the product of the mean ice thickness of the area loss due to calving and area of annual calving losses (*SI Materials and Methods*). The area enclosed between the outer boundary (ice shelf front) and the inner boundary (fracture line) over the annual interval gives the calving area. Calving areas are manually traced from coregistered pairs of consecutive August 2005–2011 Envisat ASAR image mosaics with a spatial resolution of 75 m and geolocation accuracy of 50 m (*SI Data*). Because ice shelves move forward, calving area detection requires tracing both ice shelf margin (ice front) and the fracture line in the original image (before calving) and the second image (after calving). The ice front is delineated by an automated object-oriented classification method based on watershed segmentation combined with manual modifications (*Fig. S4 A and B*). Identifying the fracture line is done manually with visual interpretation and spatial adjustment. In the case of tabular calving (*Fig. 3A*), calving area at the ice shelf front is obviously visible; in the case of calving associated with large-scale crevassing (*Fig. 3C*), surface features at the ice front of the second image can be matched with features in the original image, allowing the fracture line to be estimated (*Fig. S4 C and D*); in the other case of calving (e.g., *Fig. 3B*) where features cannot be uniquely identified, advance of the starting ice front is estimated by a flow-line method (*SI Materials and Methods*).

Basal Melt. An estimate for B is obtained by rearranging Eq. 2.

$$B = F_G + SMB - C - \frac{\Delta M}{\Delta t} \quad [3]$$

Steady-State Iceberg Calving. The steady-state iceberg calving, assuming no change of ice shelf areal extent, is the sum of iceberg calving and mass change rate due to extent change (positive for advance and negative for retreat).

$$C_{ss} = C + \frac{\Delta M_A}{\Delta t} \quad [4]$$

Steady-State Basal Melt. The steady-state basal melt, assuming no change of ice shelf thickness, is calculated as the sum of basal melt and mass change rate due to ice thickness change (positive for ice thickening and negative for ice thinning).

$$B_{ss} = B + \frac{\Delta M_H}{\Delta t} \quad [5]$$

ACKNOWLEDGMENTS. We thank M. R. van den Broeke and S. R. M. Ligtenberg for providing firm depth correction data, European Space Agency for providing Envisat ASAR data, and National Snow and Ice Data Center for distribution of other data. We thank the editor, two anonymous reviewers, T. A. Scambos, and K. C. Wang, whose comments substantially improved the manuscript. We also thank H. Huang, X. Li, F. Wang, T. Ci, T. Zhao, and M. Zhai for assistance with data processing. This research is supported by Chinese Arctic and Antarctic Administration, National Basic Research Program of China Grants 2012CB957704 and 2015CB953600; National Natural Science Foundation of China, Grants 41406211, 41176163, 41106157, and 41276188; National High-tech R&D Program of China Grants 2008AA121702 and 2008AA09Z117; Chinese Polar Environment Comprehensive Investigation & Assessment Programmes; Fundamental Research Funds for the Central Universities of China; and Young Talent fund of the State Key Laboratory of Remote Sensing Science. R.M.G. is funded by Marie Curie Actions within the European Commission Framework Programme 7, and J.N.B. was supported by National Science Foundation Grants NSF-ANT 114085 and NSF-ARC 1064535.

- Moore JC, Grinsted A, Zwinger T, Jevrejeva S (2013) Semi-empirical and process-based global sea level projections. *Rev Geophys* 51(3):484–522.
- Depoorter MA, et al. (2013) Calving fluxes and basal melt rates of Antarctic ice shelves. *Nature* 502(7469):89–92.
- Rignot E, Jacobs S, Mouginot J, Scheuchl B (2013) Ice-shelf melting around Antarctica. *Science* 341(6143):266–270.
- Dupont TK, Alley RB (2005) Assessment of the importance of ice-shelf buttressing to ice-sheet flow. *Geophys Res Lett* 32(4):L04503.
- Pritchard HD, Vaughan DG (2007) Widespread acceleration of tidewater glaciers on the Antarctic Peninsula. *J Geophys Res* 112(F3):F03529.
- Rignot E, et al. (2008) Recent Antarctic ice mass loss from radar interferometry and regional climate modelling. *Nat Geosci* 1(2):106–110.
- Holt TO, Glasser NF, Quincey DJ, Siegfried MR (2013) Speedup and fracturing of George VI Ice Shelf, Antarctic Peninsula. *Cryosphere* 7:797–816.
- Scambos TA, Hulbe CL, Fahnestock MA (2003) Climate-induced ice shelf disintegration in the Antarctic Peninsula. *Antarct Res Ser* 79:79–92.
- Rignot E, Koppes M, Velicogna I (2010) Rapid submarine melting of the calving faces of West Greenland glaciers. *Nat Geosci* 3(3):187–191.
- MacGregor JA, Catania GA, Markowski MS, Andrews AG (2012) Widespread rifting and retreat of ice-shelf margins in the eastern Amundsen Sea Embayment between 1972 and 2011. *J Glaciol* 58(209):458–466.
- Jacobs SS, Jenkins A, Giulivi CF, Dutrieux P (2011) Stronger ocean circulation and increased melting under Pine Island Glacier ice shelf. *Nat Geosci* 4(8):519–523.
- Pritchard HD, et al. (2012) Antarctic ice-sheet loss driven by basal melting of ice shelves. *Nature* 484(7395):502–505.
- Bassis JN, Jacobs SS (2013) Diverse calving patterns linked to glacier geometry. *Nat Geosci* 6(10):833–836.
- Nick FM, et al. (2013) Future sea-level rise from Greenland's main outlet glaciers in a warming climate. *Nature* 497(7448):235–238.
- Åström JA, et al. (2014) Termini of calving glaciers as self-organized critical systems. *Nat Geosci* 7:874–878.
- Joughin I, MacAyeal DR (2005) Calving of large tabular icebergs from ice shelf rift systems. *Geophys Res Lett* 32(2):L02501.
- Fricker HA, Young NW, Allison I, Coleman R (2002) Iceberg calving from the Amery Ice Shelf, East Antarctica. *Ann Glaciol* 34(1):241–246.
- Bassis JN, Fricker HA, Coleman R, Minster J-B (2008) An investigation into the forces that drive ice-shelf rift propagation on the Amery Ice Shelf, East Antarctica. *J Glaciol* 54(184):17–27.
- Scambos TA, et al. (2009) Ice shelf disintegration by plate bending and hydro-fracture: Satellite observations and model results of the 2008 Wilkins ice shelf break-ups. *Earth Planet Sci Lett* 280(1):51–60.
- Jakobsson M, et al. (2011) Geological record of ice shelf break-up and grounding line retreat, Pine Island Bay, West Antarctica. *Geology* 39(7):691–694.
- Young NW, Legresy B, Coleman R, Massom R (2010) Mertz Glacier tongue unhinged by giant iceberg. *Aust Antarct Mag* 18:19.
- Pritchard HD (2014) Bedgap: Where next for Antarctic subglacial mapping? *Antarct Sci* 26(6):742–757.
- Lambrecht A, Sandhager H, Vaughan DG, Mayer C (2007) New ice thickness maps of Filchner-Ronne Ice Shelf, Antarctica, with specific focus on grounding lines and marine ice. *Antarct Sci* 19(4):521.
- Scambos TA, Bohlander J, Shuman CA, Skvarca P (2004) Glacier acceleration and thinning after ice shelf collapse in the Larsen B embayment, Antarctica. *Geophys Res Lett* 31(18):L18402.
- Holland PR, Corr HF, Vaughan DG, Jenkins A, Skvarca P (2009) Marine ice in Larsen ice shelf. *Geophys Res Lett* 36(11):L11604.
- Kulesa B, Jansen D, Luckman AJ, King EC, Sammonds PR (2014) Marine ice regulates the future stability of a large Antarctic ice shelf. *Nat Commun* 5:3707.
- MacAyeal DR, Scambos TA, Hulbe CL, Fahnestock MA (2003) Catastrophic ice-shelf break-up by an ice-shelf-fragment-capsule mechanism. *J Glaciol* 49(164):22–36.
- McGrath D, et al. (2014) The structure and effect of suture zones in the Larsen C Ice Shelf, Antarctica. *J Geophys Res* 119(3):588–602.
- Weertman J (1973) Can a water-filled crevasse reach the bottom surface of a glacier? *Int Assoc Sci Hydrol Publ* 95:139–145.
- Thoma M, Jenkins A, Holland DM, Jacobs SS (2008) Modelling circumpolar deep water intrusions on the Amundsen Sea continental shelf, Antarctica. *Geophys Res Lett* 35(18):L18602.
- Dinniman MS, Klinck JM, Hofmann EE (2012) Sensitivity of Circumpolar Deep Water transport and ice shelf basal melt along the west Antarctic Peninsula to changes in the winds. *J Clim* 25(14):4799–4816.
- Khazendar A, Rignot E, Larour E (2009) Roles of marine ice, rheology, and fracture in the flow and stability of the Brunt/Stancomb-Wills Ice Shelf. *J Geophys Res* 114(F4):F04007.
- Larour E, Rignot E, Aubry D (2004) Modelling of rift propagation on Ronne Ice Shelf, Antarctica, and sensitivity to climate change. *Geophys Res Lett* 31(16):L16404.
- McGrath D, et al. (2012) Basal crevasses and associated surface crevassing on the Larsen C ice shelf, Antarctica, and their role in ice-shelf instability. *Ann Glaciol* 53(60):10–18.
- Vaughan DG, et al. (2012) Subglacial melt channels and fracture in the floating part of Pine Island Glacier, Antarctica. *J Geophys Res* 117(F3):F03012.
- Liu Y, et al. (2014) Detection of crevasses over polar ice shelves using Satellite Laser Altimeter. *Sci China Earth Sci* 57(6):1267–1277.